

# Optimal Networks of Future Gravitational-Wave Telescopes

Péter Raffai<sup>1,2</sup>, László Gondán<sup>2</sup>, Ik Siong Heng<sup>3</sup>, Nándor Kelecsényi<sup>2</sup>, Josh Logue<sup>3</sup>, Zsuzsa Márka<sup>1</sup>, Szabolcs Márka<sup>1</sup>

<sup>1</sup> Columbia University, Department of Physics, New York, NY 10027, USA

<sup>2</sup> Eötvös University, Institute of Physics, 1117 Budapest, Hungary

<sup>3</sup> SUPA, University of Glasgow, Glasgow, G12 8QQ, United Kingdom

E-mail: pr2200@columbia.edu

**Abstract.** We aim to find the optimal site locations for a hypothetical network of 1–3 triangular gravitational-wave telescopes. We define the following  $N$ -telescope figures of merit and construct three corresponding metrics: (a) capability of reconstructing the signal polarization; (b) accuracy in source localization; and (c) accuracy in reconstructing the parameters of a standard binary source. We also define a combined metric that takes into account the three figures of merit with practically equal weight. After constructing a geomap of possible telescope sites, we give the optimal 2-telescope networks for the four figures of merit separately in example cases where the location of the first telescope has been predetermined. We found that the optimal site locations for a second telescope based on the combined metric form a  $\pm 7^\circ$  annulus at an angular distance of  $\sim 130^\circ$  from the location of the first telescope. Based on this result we conclude that placing the first telescope to Australia provides the most options for optimal site selection when extending the network with a second instrument. We suggest geographical regions where a potential second and third telescope could be placed to get optimal network performance in terms of our figures of merit. Additionally, we use a similar approach to find the optimal location and orientation for the proposed LIGO-India detector within a five-detector network with Advanced LIGO (Hanford), Advanced LIGO (Livingston), Advanced Virgo, and KAGRA.

PACS numbers: 95.45.+i, 95.55.Ym

Submitted to: *Class. Quantum Grav.*

## 1. Introduction

Modern gravitational-wave (GW) detectors are state-of-the-art interferometers with arm lengths typically on the kilometer scale. The most advanced network of such instruments so far consists of the two detectors of the Laser Interferometer Gravitational-wave Observatory (LIGO) [1] at Hanford (Washington, USA) and at Livingston (Louisiana, USA), both having 4 km long arms, and the Virgo detector at Cascina (Italy) [2], having a 3 km arm length. All three detectors are currently undergoing major upgrades until they will come back online around 2014-2017 as a network of second generation GW detectors, named as Advanced LIGO [3] and Advanced Virgo [4], respectively.

Two additional L-shaped detectors are proposed to become operational shortly after 2018, and will join the network of second generation detectors: the LIGO-India in India [5], and the KAGRA detector in Japan [6], with 4 and 3 km long arms, respectively. The KAGRA detector is to be constructed in the Kamioka mine, which already sets the location and orientation of this future instrument. However, the site location and the orientation of the arms of LIGO-India have not yet been finalized. This provides an opportunity to suggest both based on purely scientific figures of merit.

According to source models, the detection of GWs is expected shortly after the second generation GW detectors start taking data with their proposed nominal sensitivity [7]. This opens up the era of *GW astronomy*, where the expected common detection of GWs provides an opportunity for observing distant sources and yet unexplored physical processes, making GW detectors powerful tools of astronomical research, similar to electromagnetic telescopes. To emphasize this major shift in the functionality of these kilometer-scale interferometers, we often use the term *GW telescopes* to refer to future GW detectors during and beyond the second generation era. Since the results in this paper correspond to such future instruments, we are going to use the term *GW telescopes* to refer to them, and keep the term *GW detectors* for instruments that primarily aim to make the first detection of GWs. In this terminology, advanced (second generation) interferometers should only be categorized as GW telescopes after they have undergone the expected shift from the first detection to the routine detection era.

Precision GW astronomy requires GW telescopes even beyond the expected sensitivities of second generation interferometers, extending also at low frequencies. The Einstein Telescope (ET) project [8] is a good example that aims to pioneer novel design configurations, construction methods, and operational techniques, to overcome the limitations of advanced interferometers in GW astronomy. The final goal of the ET project is to provide a baseline for the future construction of a *third generation* GW telescope. This, according to the conceptual document [9], will consist of three interferometers (single-interferometer design) or interferometer *pairs* (xylophone design) with 10 km long arms, built underground in a way to form an equilateral triangle shape. The ET is aspiring to have a noise level about one order of magnitude below the noise floor of Advanced LIGO in its most sensitive range, and extend sensitivity at lower

frequencies [10]. This would make the ET capable of observing GW sources at distances of even up to several gigaparsecs, depending on the source type [9].

GW telescopes are not equally sensitive to GWs coming from different sky directions. Beyond the scientific advantages of improved sensitivity and of having multiple interferometers at one telescope site, the equilateral triangle geometry makes the directional sensitivity of such a GW telescope cylindrically symmetric around the symmetry axis of the triangle for both GW polarizations [11]. In practice, this means that all the scientific figures of merit we can define in terms of GW detection will be independent from how the triangle is oriented at a given geographical position. For a network of such GW telescopes, the corresponding figures of merit will only depend on the geographical positions of the individual GW telescopes relative to each other.

The scientific advantages of the geometrical design proposed by the ET project sets a long term model for future GW telescope development in the third-generation era and possibly even beyond. Therefore to preserve the generality of our discussions, from now on we will use the term *Delta telescope* ( $\Delta$ -telescope) to refer to a future or hypothetical GW telescope that consists of three  $\mathcal{O}(10 \text{ km})$  scale interferometers sharing the same site and forming an equilateral triangle shape, similarly to the proposed design for the ET. The sketch of a  $\Delta$ -telescope is shown in figure 1.

Although there are some promising site candidates based on local noise background measurements [9], the future geographical position of the first  $\Delta$ -telescope is still unknown. Beyond the expected local noise background, one can also consider figures of merit of a *network* of GW telescopes when selecting the best site candidates for any number of future telescopes. In doing so, we should first consider what type of GW telescopes we should take into account in a future network that will include at least one  $\Delta$ -telescope.

We consider a first  $\Delta$ -telescope that provides an improvement over the second-generation GW telescopes in the limiting sensitivity by more than a factor of 10 over their entire frequency band [10]. This yields a far better detector performance, and different physics to be explored [10, 12]. As such an instrument becomes operational (after 2020 at earliest [9]), the second-generation GW telescopes with less than 10% sensitivity and 0.1% explorable volume will become irrelevant as coherent detection partners. Therefore we only consider  $N$ -telescope networks here where *all* the nodes are  $\Delta$ -telescopes, when exploring the best site locations based on  $N$ -telescope figures of merit.

In case of a single  $\Delta$ -telescope, the first figure of merit that we need to take into account when choosing the site location from an allowed set of locations is the expected noise background caused by local environmental effects. However, when building a network of more than one  $\Delta$ -telescope, the selection of the first site already severely restricts the optimal location for the second (and third, fourth, etc.) telescope, based on the  $N$ -telescope figures of merit. By not taking this into account when selecting the site for the first telescope, one might get into a situation where the set of site candidates for the additional detectors has already narrowed down to options that are sub-optimal

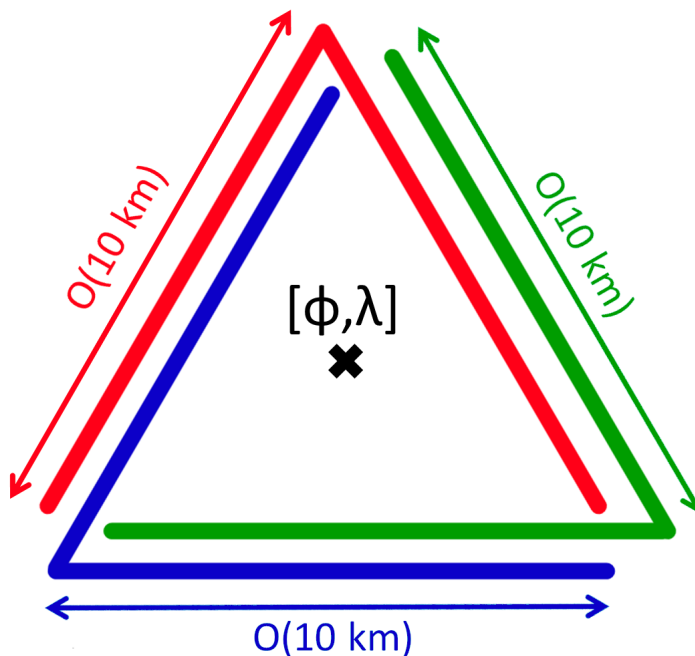


Figure 1: The sketch of a hypothetical *Delta telescope* ( $\Delta$ -telescope). The instrument consists of three identical interferometers (single-interferometer design) or interferometer pairs (xylophone design) with  $\mathcal{O}(10 \text{ km})$  long arms. The opening angle between the arms of each interferometer is  $60^\circ$ , and the interferometers are oriented such that they form an equilateral triangle shape. The center of the triangle (marked with  $\times$ ) is placed to a geographical position represented by  $[\Phi, \lambda]$  latitude and longitude coordinates, respectively. Note, that this is the baseline design geometry proposed by the ET design document [9].

in terms of the  $N$ -telescope figures of merit. Therefore even though there has not been any published plans yet to construct more than one  $\Delta$ -telescopes, it is critical to keep the door open for a future extension to  $N > 1$   $\Delta$ -telescopes and explore the best site candidates for a network of multiple  $\Delta$ -telescopes. Thus, we emphasize that the results based on  $N$ -telescope figures of merit should be taken into account in the site selection of the first  $\Delta$ -telescope, which we treat as the *primary* element constructed in a possible future network of GW telescopes.

In this paper, we suggest optimal locations for 1 – 3  $\Delta$ -telescopes from a set of possible sites chosen with respect to basic geographic limitations (e.g. availability of solid ground; elevation of the site; etc.) and expected noise levels from local environmental effects (such as near-coastal microseism and human activity). In the analysis, we intentionally disregard geopolitical considerations to allow for best science type optimization. The optimization is carried out in terms of three different  $N$ -telescope figures of merit, and in terms of a combined example metric that takes into account the three figures of merit with practically equal weight. In the optimization, for simplicity, we assume that all  $\Delta$ -telescopes in the network are identical and have the

same sensitivity curve.

Additionally, we use the same approach to find the optimal location and orientation for the proposed LIGO-India detector within a five-detector network with Advanced LIGO (Hanford), Advanced LIGO (Livingston), Advanced Virgo, and KAGRA. In this case, again for simplicity, we assumed that these L-shaped detectors have practically the same noise levels. In the frequency band around 100 Hz where these detectors will have their lowest level of noise, this approximation is reasonably accurate (e.g. see figure 5. in [9]).

The paper is organized as follows. In section 2 we discuss how the set of acceptable site locations were chosen from a geographical map of the world. In section 3 we introduce three  $N$ -telescope figures of merit together with the corresponding metrics, and a combined metric defined in the three-dimensional metric space. In section 4, we give the optimal 2-telescope networks for the four figures of merit separately in example cases where the location of the first telescope has been predetermined. We also suggest geographical regions in section 4 where the first three telescope in a network should be placed to get optimal network performance in terms of our figures of merit, and to provide the most options for optimal site selection when extending the network with an additional instrument. Section 5 discusses the results of the site location and orientation optimization for the future LIGO-India detector. Finally, we summarize and discuss our results in section 6.

## 2. Selection of possible telescope sites

In the process of constructing a set of possible site locations for a future GW telescope, we filtered out geographical positions where either the construction of kilometer-scale interferometers would be unfeasible, or where we expect to have permanent local noise sources that would strongly limit the scientific performance of the telescope during observational runs.

We started our selection process with a cylindrically projected map of the world, where the oceanic surfaces have already been filtered out. We removed the polar regions from the map due to the harsh weather conditions that would make the construction and operation of a GW telescope unfeasible. We also subtracted all the continental lakes from our map. Finally, we applied a cut at an elevation limit of 2000 meters above sea level, due to the limited accessibility of such places.

We applied two additional filters that were based on considerations of local noise sources. Due to the high level of excess near field seismic noise caused by oceanic waves clashing to the continental shelf, we removed a  $\sim 100$  km wide zone along the coastlines of continents and islands. To exclude areas that are permanently affected by intense human activity that leads to an increased level of gravity gradient background, we used a high-resolution image of Earth's city lights from the Visible Earth Catalog of the National Aeronautics and Space Administration (NASA) [13]. By removing the high-intensity pixels of the city lights map from our map of site candidates, we excluded both

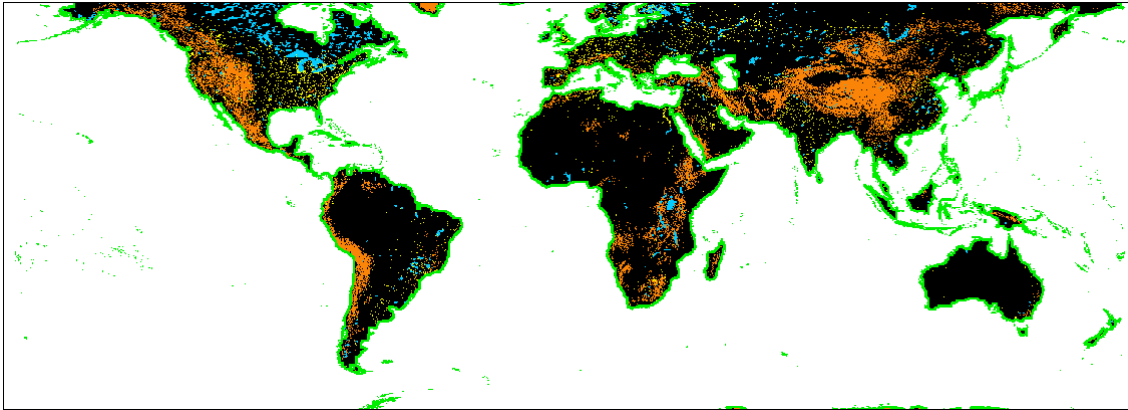


Figure 2: The map of acceptable regions for the construction of a future  $\Delta$ -telescope (black), together with the excluded geographical areas: oceanic surfaces (white), continental lakes (blue), locations at elevations higher than 2000 m above sea level (brown), near-coastal regions within  $\sim 100$  kilometers (green), and urban areas (yellow). The remaining locations (black) were discretely sampled and were used as a set of acceptable telescope sites for our numerical analysis.

the urban areas and the most heavily used traffic roads.

The resulting set of acceptable sites, together with the excluded geographical areas are visualized in figure 2. The remnant geographical areas were discretely sampled to get a sub-sample of locations where the geographical positions are  $\sim 300$  km away from each other. The resulting 1525 locations were treated as the set of acceptable sites for  $\Delta$ -telescopes. Note, that future analyses with additional constraints and refinements might nuance the local selection of acceptable sites, but will not affect the global picture we are about to present here.

### 3. $N$ -telescope figures of merit and metrics

In this section we introduce the figures of merit that we used to evaluate the scientific potential of the different configurations of a  $\Delta$ -telescope network. Our framework in many ways is similar to the ones introduced in [14] and in [15].

As discussed in section 1, the figures of merit for a network of  $\Delta$ -telescopes are independent from the orientation of the individual telescopes. We also pointed out that the horizon distances of  $\Delta$ -telescopes for the targeted GW source types are in the order of many gigaparsecs, in which the distribution of matter can be approximated as homogeneous and isotropic. Due to the rotation of Earth and its orbital motion around the Sun, the directional sensitivity of a ground-based GW telescope changes with time towards the different directions in the galactic frame. By taking into account all these effects, as a first approximation, we only need to consider the positions of the GW telescopes in the network *relative* to each other, and use all-sky averaged figures of merit to characterize the network.



As an alternative, one can configure a network such as to maximize the observational time with the highest directional sensitivity towards a certain sky direction. This sky direction could be chosen based on known inhomogeneities or anisotropies in the mass distribution of the local Universe. However, in this work we optimized the network configurations based on all-sky averaged figures of merit, leaving the local mass distribution as the scope of a follow-up paper.

In the following subsections, we are going to introduce three all-sky averaged figures of merit together with the corresponding metrics to characterize the different configurations of  $\Delta$ -telescope networks. Additionally, we are going to discuss why it is unnecessary to consider the average directional sensitivity (or *reach* [14]) of the network as a fourth figure of merit. We summarize our figures of merit and metrics at the end of this section, in table 1.

### 3.1. Capability of reconstructing the signal polarization

Interferometric GW telescopes sense the change in the distance between their test masses along the lines of the interferometer arms. Therefore in order to model the strain output of a telescope for a GW signal arriving from a given sky direction, one must project the GW strain to the reference frame set by the interferometer arms. The projection can be given as a linear combination of the  $+$  and  $\times$  polarization components of the incoming GW signal, where the linear factors,  $F_+$  and  $F_\times$  (ranging from 0 to 1, and called "antenna factors") depend on the sky direction relative to the interferometer arms, and on the angle that sets the orientation of the frame in which the two polarizations are defined. This frame is called the "polarization frame", while the corresponding angle is called the "polarization angle", and conventionally denoted by  $\Psi$ .

By choosing a  $\Psi$  polarization angle, one can plot the antenna factors for any ground-based interferometers as functions of the different sky directions given by  $\Phi$  latitude and  $\lambda$  longitude coordinates in the Earth-centered coordinate system. These two-dimensional plots are called "antenna patterns", and they can be constructed for a network of  $N$   $\Delta$ -telescopes by using the same polarization angle for all interferometers, and calculating the root-mean-square average of the  $+$  and  $\times$  antenna factors for the  $3N$  individual interferometers:

$$F^{\text{network}} = \sqrt{\frac{F_1^2 + F_2^2 + F_3^2 + \dots + F_{3N}^2}{3N}}. \quad (1)$$

Here the  $F$  antenna factors can either all correspond to the  $+$  or to the  $\times$  signal polarization. Also, for any number of interferometers and for any sky directions one can always choose the polarization angle such that  $F_+$  is maximized, and  $F_\times$  is minimized, and therefore  $F_+ \geq F_\times$ . This special polarization frame is called the Dominant Polarization Frame (DPF) (see [16] and [17] for more details). Normally, when constructing the DPF for multiple interferometers, one needs to take into account their noise levels relative to each other in the frequency band of interest [17]. However when

all interferometers are identical (as in the case of  $N$   $\Delta$ -telescopes), this consideration is not necessary.

The sensitivity of a network of telescopes towards a chosen direction is usually characterized by the root-mean-square average of  $F_+^{\text{network}}$  and  $F_\times^{\text{network}}$ . However, depending on the network configuration, the ratio of  $F_\times^{\text{network}}$  and  $F_+^{\text{network}}$  within this average can have any value from zero to one (note that  $F_+^{\text{network}} \geq F_\times^{\text{network}}$  is always true in the DPF). This ratio towards a given sky direction characterizes the relative network sensitivity to the two GW polarizations, and is conventionally called the *network alignment factor* [16]. The value of this factor determines the ratio of the signal-to-noise ratios from the two GW polarization components, assuming that in average their sum-square energies are the same.

Having a  $F_\times^{\text{network}}/F_+^{\text{network}}$  ratio equal to 1 in the DPF means that the network is equally sensitive to both polarizations of a GW signal incoming from the given direction. On the other hand, if the  $F_\times^{\text{network}}/F_+^{\text{network}}$  ratio is significantly lower than 1 in the DPF, that means that the network will be relatively insensitive to the  $\times$  polarization component of the signal ( $\times$  being defined in the DPF), and thus the network will have a limited capability of detecting the  $\times$  component of a GW signal incoming from the given direction. Since in order to reconstruct the polarization of a GW signal, we need to be able to detect and reconstruct the energy content of the signal for both polarizations,  $F_\times^{\text{network}}/F_+^{\text{network}} \approx 1$  can be interpreted as optimal in reconstructing the signal polarization for the given sky direction, provided that the overall signal strength is sufficient. Therefore to characterize a telescope network configuration in terms of its capability of reconstructing the signal polarization, we can use the  $|F_+^{\text{network}} - F_\times^{\text{network}}|^2$  quantity averaged over all sky directions:

$$I = \left( \frac{1}{4\pi} \oint |F_+^{\text{network}}(\Phi, \lambda) - F_\times^{\text{network}}(\Phi, \lambda)|^2 d\Omega \right)^{-\frac{1}{2}} \quad (2)$$

where  $\Phi$  and  $\lambda$  are the latitude and longitude coordinates of the different sky directions defined in the Earth-centered coordinate system, and  $d\Omega = \cos\Phi d\Phi d\lambda$  is the infinitesimal solid angle towards the  $[\Phi, \lambda]$  direction. If we want to construct an optimal network of telescopes by maximizing its capability of reconstructing the signal polarization, we should minimize the all-sky average of the  $|F_+^{\text{network}} - F_\times^{\text{network}}|^2$  difference. As shown by Eq. 2, the  $I$  metric is defined in a way that it should be *maximized* instead.

### 3.2. Accuracy in source localization

Transient GW signals that we expect to detect with a future  $\Delta$ -telescope will have a duration of  $\mathcal{O}(1 \text{ ms} - 1000 \text{ sec})$  in the sensitive band. For such signals, the localization of the source in the sky can be achieved by triangulation based on the times of detection of the incoming signal with multiple interferometers [18].

The detection times can only be measured with an accuracy that is directly proportional to the signal-to-noise ratio, and thus to one over the strain noise level of the



interferometer within the bandwidth of the signal [18]. This uncertainty in the detection time measurement can be translated into uncertainty in the source localization for the signal. However, when the goal is to compare the accuracy in source localization for different configurations of  $N$  identical telescopes, the noise levels of the interferometers do not need to be taken into account when constructing a metric.

Since the triangulation is based on the *differences* between the detection times, the accuracy in source localization also depends on the distances between the telescope sites along the line-of-sight to the GW source. If we want to maximize the average accuracy of source localization towards all sky directions, we must place the telescopes of the network as far away from each other as possible in the three dimensional space. For a 2-telescope network, this makes the distance between the two telescopes an obvious choice for a metric to be maximized. For a 3-telescope network, it is the *area* of the triangle formed by the three telescopes, that should be maximized (e.g. see Eq.(1) in [19]). In order to have the same units for the 2- and 3-telescope metric, we use the *square* of the distance between the telescopes as the metric in the 2-telescope case. In both cases, we denote the metric corresponding to the potential of the network in source localization as  $D$ .

In case of the LIGO-India tests, where the network consists of  $N = 5$  telescopes, we choose  $D$  to be the area of the triangle with the largest area among the triangles formed by all possible combinations of three telescopes in the network. Thus, as a simplification, we characterize the  $N = 5$  network with the  $D$  metric value of its best  $N = 3$  sub-network in terms of accuracy in source localization.

### 3.3. Accuracy in reconstructing the parameters of a standard binary source

The most promising candidates of GW emission observable by future GW telescopes are binary systems of black holes (BHs) and/or neutron stars (NSs). Based on the models of such systems and the proposed sensitivity curve for ET, future  $\Delta$ -telescopes should be able to detect the GW emission of these binaries up to several or several tens of gigaparsecs, depending on the total mass of the system [9].

The waveforms of the GW signals from these sources are known with a relatively high accuracy from post-Newtonian calculations even in cases when the spins of the binary components are not negligible [20, 21]. This makes binary systems of BHs and/or NSs *standard sources* in the sense that they can be used to characterize the capabilities of a GW telescope or a network of GW telescopes in terms of distance reach and accuracy in source parameter reconstruction.

In case of a circular binary of spinless compact stars, the typical parameters to be reconstructed from the GW waveform are the chirp mass of the system and the distance of the source [20]. The alignment of the orbital plane relative to the line-of-sight is reconstructed from the relative power in the  $+$  and  $\times$  components of the incoming signal [20], and thus the performance of the telescope network in terms of this is already being tested by the  $I$  metric (see section 3.1).

If we choose a configuration of  $N$  identical  $\Delta$ -telescopes, we can use the Fisher matrix method [22] to calculate the chirp mass and source distance reconstruction errors for a standard GW source. The source that we chose is an inspiraling binary of spinless neutron stars, each having a mass of  $1.4M_{\odot}$ , placed to a distance of 1 Gpc from Earth, and aligned such that the orbital plane is always perpendicular to the line-of-sight. For this standard source, the sensitivity curves for the single-interferometer (ET-B in [9]) and the xylophone designs (ET-C or ET-D in [9]) are practically the same in the frequency band of the emitted GW signal, and thus the results are independent from the specific sensitivity curve we choose from these three options (we used ET-B in our calculations). Also, as we pointed out earlier, a future  $\Delta$ -telescope should have no problem detecting such a binary source at a 1 Gpc distance, and reconstructing its chirp mass.

Generally the orbit of an inspiraling binary is elliptical, and the principal axes of the ellipse give a preferred polarization basis [20, 23]. However, when the line-of-sight is perpendicular to the orbital plane, the components of the base vectors as defined in [20] become singular. Since the incoming GW signal is circularly polarized in our case, we can choose any two orthogonal vectors as polarization bases perpendicular to the line-of-sight, and resolve the singularity. In choosing such a polarization basis, as an approximation, we neglected the change in the direction of the line-of-sight throughout the time while the signal is within the sensitive band of the  $\Delta$ -telescope.

Using the waveform of the spinless binary in the Newtonian approximation [20], we calculated the components of the Fisher information matrix [24] for each single interferometer, and summed it up for all the interferometers in the  $\Delta$ -telescope sites. We found that it is unnecessary to construct a separate metric based on chirp mass and source distance reconstruction errors, because the results are the same when we compare the different network configurations using the two metrics. Thus we chose a metric that is based on chirp mass reconstruction error only. We also found that the chirp mass reconstruction errors only slightly depend on the off-diagonal elements of the Fisher information matrix (the results with and without the off-diagonal elements are within less than 0.5%). Thus for simplicity, we only used the diagonal elements of the Fisher information matrix when calculating the chirp mass reconstruction errors.

The chirp mass reconstruction error,  $\sigma_{\mathcal{M}}$ , depends on the source location relative to the positions of the telescope sites ( $\sigma_{\mathcal{M}} = \sigma_{\mathcal{M}}(\Phi, \lambda)$ ). In order to identify the best telescope network configuration, we used the all-sky average of this quantity:

$$R = \left( \frac{1}{4\pi} \oint \sigma_{\mathcal{M}}^2 d\Omega \right)^{-\frac{1}{2}} = \langle \sigma_{\mathcal{M}}^2 \rangle^{-\frac{1}{2}}, \quad (3)$$

so that maximization of  $R$  should lead to the minimum uncertainty of the reconstructed chirp mass averaged to the whole sky.

### 3.4. Why we should not care about the directional sensitivity of the network

One way to characterize the directional sensitivity of a telescope network is to calculate the mean square of its combined antenna factors for the  $+$  and  $\times$  polarizations toward

the different sky directions. This measure will be independent from the polarization angle for any geometry of the interferometer arms, and thus independent from the orientations of the individual telescopes. By calculating the root-sum-square average of this quantity for the whole sky, we get a metric that characterizes the average directional sensitivity of the network for the whole sky, a.k.a. the average *reach* of the network [14]. For a network of  $N$   $\Delta$ -telescopes consisting of  $3N$  interferometers, the metric is defined as:

$$X = \sqrt{\frac{1}{4\pi} \oint \frac{F_+^2(\Phi, \lambda) + F_\times^2(\Phi, \lambda)}{3N} d\Omega}, \quad (4)$$

where  $F_+ = F_+^{\text{network}}$  and  $F_\times = F_\times^{\text{network}}$ , both given in the DPF. Due to Eq.1, the integral in Eq.4 can be split to  $3N$  integrals, each corresponding to a single interferometer in the network, and the integrals can be calculated individually. The value of  $X$  will therefore never depend on the configuration of how the  $N$  telescopes in the network are arranged, even if the interferometers have a different geometry from the interferometers in a  $\Delta$ -telescope. Even though by using a different network configuration we get a different *shape* for the combined antenna pattern, the all-sky integral of that surface will be the same for all configurations. This practically means, that by choosing a different configuration, we might lose sensitivity toward certain directions, but at the same time we increase the sensitivity of the network toward other directions. The net effect is that the  $N$ -telescope network will be able to cover the same volume of the local Universe, which is good enough in our case when we assume that the accessible Universe is homogeneous and isotropic. Thus, it is unnecessary to include the  $X$  metric in our optimization procedure, and we can use only the other three metrics that we defined, denoted as  $I$ ,  $D$ , and  $R$ . Nevertheless, for future publications when targeted science is considered, a metric characterizing the directional sensitivity of the network, as well as the time evolution of cosmic reach will be important.

### 3.5. The combined metric

The three metrics we described so far,  $I$ ,  $D$ , and  $R$ , together define a three dimensional metric space. For each  $N$ -telescope configurations, we can calculate the corresponding metric values, and identify a spatial point in this space using the metric values as coordinates. The goal of the optimization process for the individual metrics is to find the configuration of  $N$  telescopes that corresponds to the highest values of  $I$ ,  $D$ , and  $R$ , respectively, from a number of Monte-Carlo trials. This is equivalent to the goal of finding the most distant data points in the metric space along the three dimensions, separately. From now on we denote these highest values of the individual metrics that we actually find in our sample of different  $N$ -telescope configurations as  $I_{\text{max}}$ ,  $D_{\text{max}}$ , and  $R_{\text{max}}$ , respectively.

The optimal configuration of an  $N$ -telescope network in a combined metric would be the one for which all the corresponding metric values are maximal within the sample.

Table 1: The figures of merit and their corresponding metrics used in the optimization of  $N$ -telescope configurations. For detailed descriptions, see section 3.

Figure of merit	Metric	Metric description
Polarization reconstruction	$I$	$\left(\frac{1}{4\pi} \oint  F_+^{\text{network}}(\Phi, \lambda) - F_\times^{\text{network}}(\Phi, \lambda) ^2 d\Omega\right)^{-\frac{1}{2}}$
Source localization (N=2)	$D$	Square of the distance between the telescopes
Source localization (N=3)	$D$	Area of the triangle formed by the telescopes
Source localization (N=5)	$D$	Area of the $N = 3$ sub-network with highest $D$
Source parameter reconstruction	$R$	$\left(\frac{1}{4\pi} \oint \sigma_{\mathcal{M}}^2 d\Omega\right)^{-\frac{1}{2}} = \langle \sigma_{\mathcal{M}}^2 \rangle^{-\frac{1}{2}}$
Combined metric	$C$	$\sqrt{\left(\frac{I}{I_{\max}}\right)^2 + \left(\frac{D}{D_{\max}}\right)^2 + \left(\frac{R}{R_{\max}}\right)^2}$

Unfortunately, due to the competing nature of the three metrics, there is no such configuration, thus, we need to construct a combined metric for such a generalized optimization process, where the three individual metrics are combined with specific weights.

In our analysis, we did not want to favor any of the three metrics specifically, therefore we normalized the metric values with  $I_{\max}$ ,  $D_{\max}$ , and  $R_{\max}$ , respectively. This makes all the metric values dimensionless, and somewhat comparable with each other in nature. Using this, the combined metric we defined was:

$$C = \sqrt{\left(\frac{I}{I_{\max}}\right)^2 + \left(\frac{D}{D_{\max}}\right)^2 + \left(\frac{R}{R_{\max}}\right)^2}. \quad (5)$$

Specific astronomic searches may require different weighting factors, given our initial goal, we used equal weights.

#### 4. Optimal networks of $\Delta$ -telescopes

We carried out an optimization procedure in three example cases where the location of the first  $\Delta$ -telescope was predetermined and a second telescope ranges over the set of 1524 acceptable sites (see section 2). In the three example cases the location of the first telescope site was chosen to be  $[\Phi_A, \lambda_A] = [48.5^\circ, 18.7^\circ]$  in Europe (Example A),  $[\Phi_B, \lambda_B] = [38.9^\circ, -98.4^\circ]$  in North America (Example B), and  $[\Phi_C, \lambda_C] = [19.6^\circ, 78.0^\circ]$  in India (Example C).

We then chose a location for the second  $\Delta$ -telescope from the set all 1524 acceptable sites, and calculated the values of the  $I$ ,  $D$ , and  $R$  metrics (see section 3) for the corresponding 2-telescope network. The resulting set of  $I$ ,  $D$ , and  $R$  values were then normalized with the highest value of the three metrics among the sample of 1524 elements, denoted as  $I_{\max}$ ,  $D_{\max}$ , and  $R_{\max}$ , respectively. The  $I/I_{\max}$ ,  $D/D_{\max}$ , and  $R/R_{\max}$  ratios (given in percentages) are shown in figure 3 for Example A (Europe), in figure 4 for Example B (USA), and in figure 3 for Example C (India).

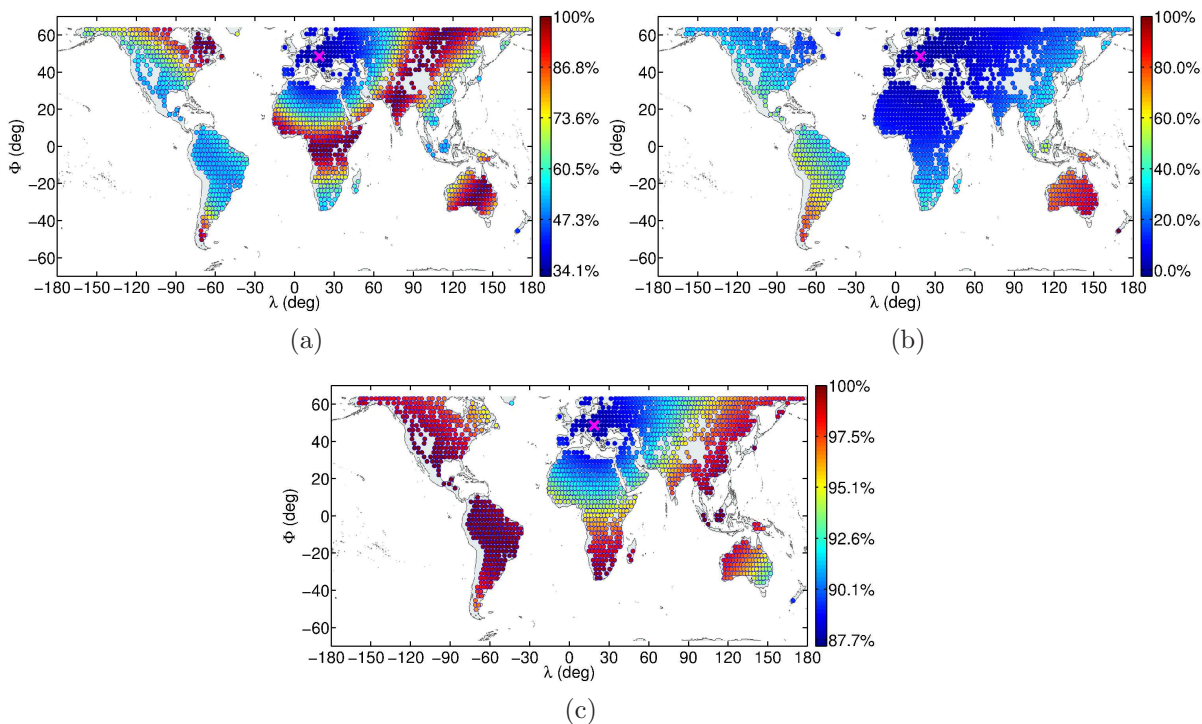


Figure 3: The colormaps of normalized metric values that we get for a network of two identical  $\Delta$ -telescopes in the case when the first telescope is placed to  $[\Phi_A, \lambda_A] = [48.5^\circ, 18.7^\circ]$  in Europe, and the location of the second telescope is chosen from the set of acceptable sites described in section 2. Each circle in the maps corresponds to one of the 1524 site locations, while their colors represent the  $I/I_{\max}$  (a),  $D/D_{\max}$  (b), or  $R/R_{\max}$  (c) values, given in percentages, where the "max" indices correspond to the highest values of the three metrics within the samples of 1524 elements.

Using the known  $\{I, D, R\}/\{I, D, R\}_{\max}$  ratios, we calculated the  $C$  metric (see section 3.5) for all the 1524 different 2-telescope configurations, and for all three example cases. We again normalized the resulting  $C$  values with the highest value in the sample,  $C_{\max}$ , and visualized the  $C/C_{\max}$  values (given in percentages) for the different configurations in figure 6 for Example A (Europe), in figure 7 for Example B (USA), and in figure 8 for Example C (India).

Based on the colormaps shown in figure 6, figure 7, and figure 8, we found that the optimal site locations for a second telescope based on the combined ( $C$ ) metric always form a  $\pm 7^\circ$  annulus at an angular distance of  $\sim 130^\circ$  from the location of the first telescope. This empirical result provided an opportunity to associate the number of acceptable sites within this annulus to all the 1525 acceptable sites that can be used as geographical locations for the first element in an optimal 2-telescope network. The resulting values, shown in figure 9, measure the number of different optimal 2-telescope configurations that can be achieved by using a given location as the base for the first  $\Delta$ -telescope in the network. As figure 9 shows, placing the first telescope in Australia



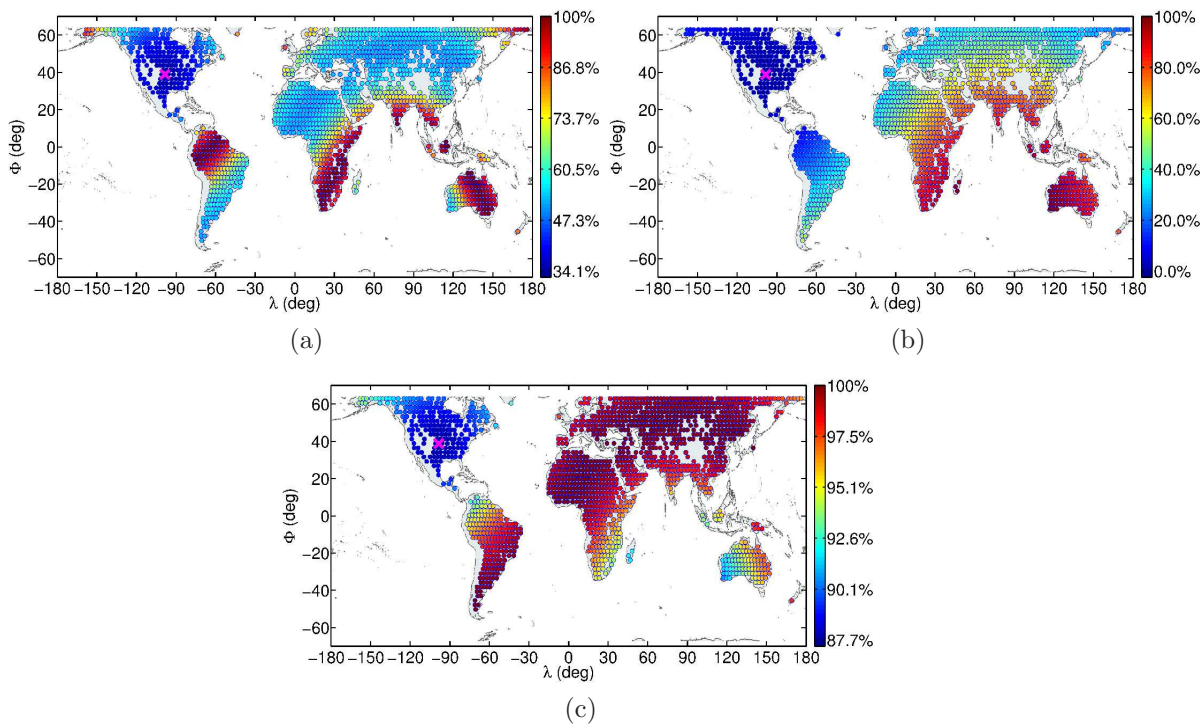


Figure 4: The colormaps of normalized metric values that we get for a network of two identical  $\Delta$ -telescopes in the case when the first telescope is placed to  $[\Phi_B, \lambda_B] = [38.9^\circ, -98.4^\circ]$  in North America, and the location of the second telescope is chosen from the set of acceptable sites described in section 2. Each circle in the maps corresponds to one of the 1524 site locations, while their colors represent the  $I/I_{\max}$  (a),  $D/D_{\max}$  (b), or  $R/R_{\max}$  (c) values, given in percentages, where the "max" indices correspond to the highest values of the three metrics within the samples of 1524 elements.

provides the most options for optimal site selection when extending the network with a second instrument.

The  $\pm 7^\circ$  annulus of optimal sites in the case when the first  $\Delta$ -telescope is placed to a geographical position of  $[\Phi, \lambda] = [-35.8^\circ, 146.9^\circ]$  in Australia is shown in figure 10. We suggest that the site location for the second telescope should be chosen from within this annulus if the first  $\Delta$ -telescope is placed to  $[\Phi, \lambda] = [-35.8^\circ, 146.9^\circ]$ . Note, that placing the first  $\Delta$ -telescope of the network to any of the acceptable sites within the annulus would result with  $[\Phi, \lambda] = [-35.8^\circ, 146.9^\circ]$  being in the annulus of optimal sites for the second  $\Delta$ -telescope.

By setting the location of the first  $\Delta$ -telescope in the network to be in Australia, and choosing a site for the second  $\Delta$ -telescope in the network from the corresponding  $\pm 7^\circ$  annulus, we can rerun the optimization procedure for a 3-telescope network with these two predetermined site locations, similarly to the previous cases of 2-telescope networks with the first site locations predetermined.

As a first example for a 3-telescope network (Example D), we chose one site at



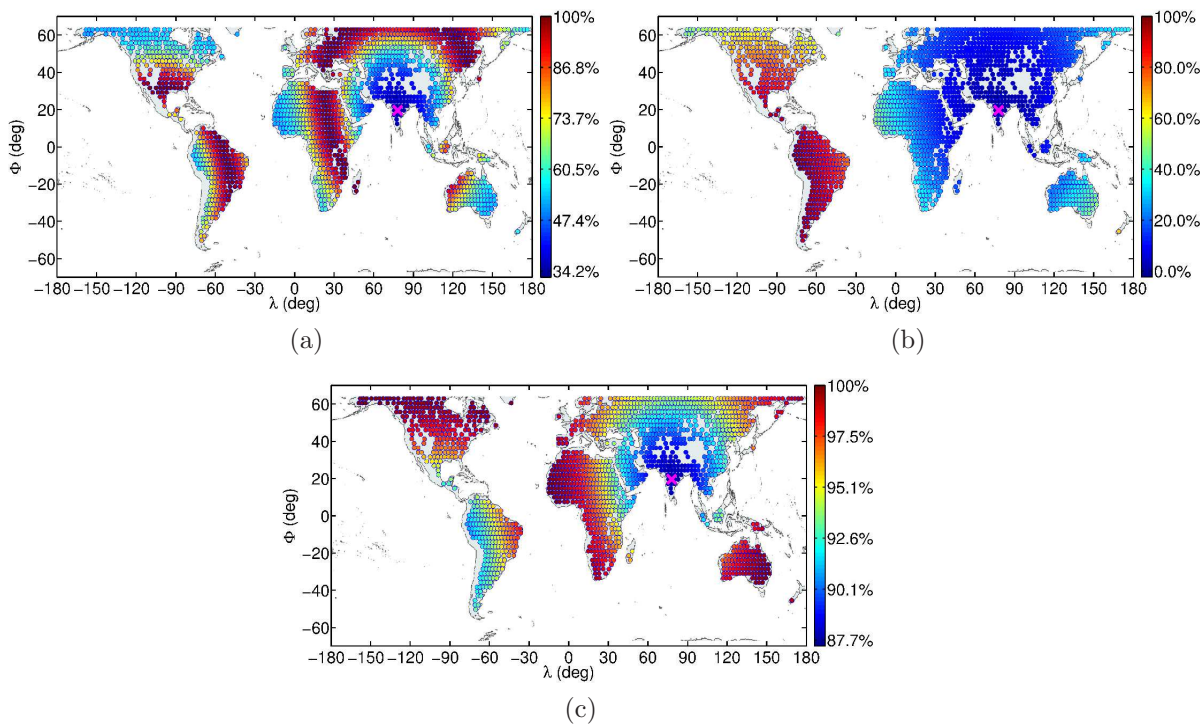


Figure 5: The colormaps of normalized metric values that we get for a network of two identical  $\Delta$ -telescopes in the case when the first telescope is placed to  $[\Phi_C, \lambda_C] = [19.6^\circ, 78.0^\circ]$  in India, and the location of the second telescope is chosen from the set of acceptable sites described in section 2. Each circle in the maps corresponds to one of the 1524 site locations, while their colors represent the  $I/I_{\max}$  (a),  $D/D_{\max}$  (b), or  $R/R_{\max}$  (c) values, given in percentages, where the "max" indices correspond to the highest values of the three metrics within the samples of 1524 elements.

$[\Phi_{D1}, \lambda_{D1}] = [-35.8^\circ, 146.9^\circ]$  in Australia, and one site at  $[\Phi_{D2}, \lambda_{D2}] = [38.9^\circ, -98.4^\circ]$  in North America. The resulting plots of  $\{I, D, R\}/\{I, D, R\}_{\max}$  ratios, given in percentages, are shown in figure 11. As shown in the  $C/C_{\max}$  ratio plot in figure 12, the optimal location for a third telescope in this network would either be in Central Africa or in the North-Central region of South America.

As a second example for a 3-telescope network (Example E), we chose one site at  $[\Phi_{E1}, \lambda_{E1}] = [-26.2^\circ, 139.2^\circ]$  in central Australia, and one at  $[\Phi_{E2}, \lambda_{E2}] = [48.5^\circ, 18.7^\circ]$  in Europe. The  $\{I, D, R\}/\{I, D, R\}_{\max}$  ratios, given in percentages, are shown in figure 13, while the  $C/C_{\max}$  ratios, also given in percentages, are shown in figure 14. The optimal locations for the third telescope in this case are in West Argentina and in West-Central Africa, based on the  $C$  metric.

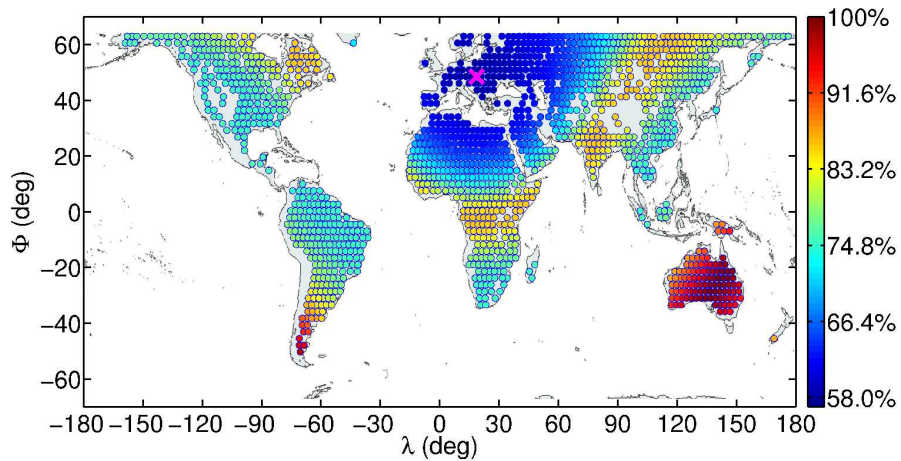


Figure 6: The colormap of  $C/C_{\max}$  values for 1524 different network configurations of two identical  $\Delta$ -telescopes, where  $C_{\max}$  is the highest value of the combined metric within the sample of 1524 elements. The location of the first telescope was chosen to be at  $[\Phi, \lambda] = [48.5^\circ, 18.7^\circ]$  (marked by  $\times$ ), and the location of the second telescope was chosen from the set of acceptable sites described in section 2.

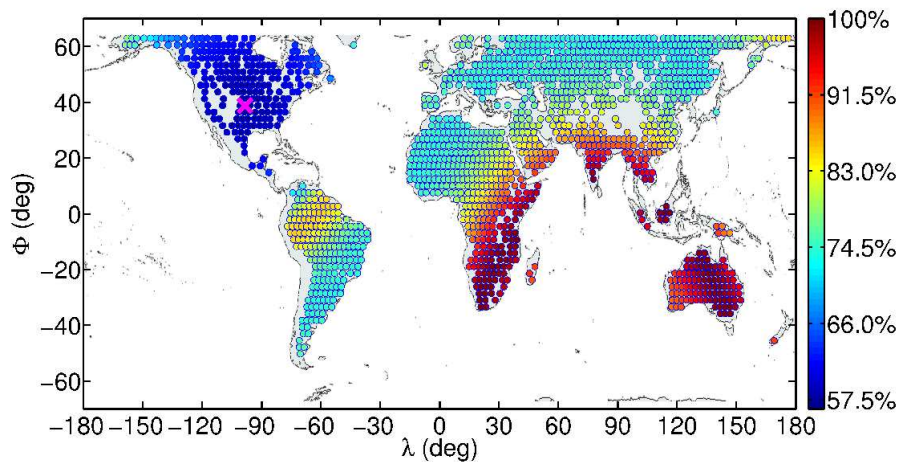


Figure 7: The colormap of  $C/C_{\max}$  values for 1524 different network configurations of two identical  $\Delta$ -telescopes, where  $C_{\max}$  is the highest value of the combined metric within the sample of 1524 elements. The location of the first telescope was chosen to be at  $[\Phi, \lambda] = [38.9^\circ, -98.4^\circ]$  (marked by  $\times$ ), and the location of the second telescope was chosen from the set of acceptable sites described in section 2.

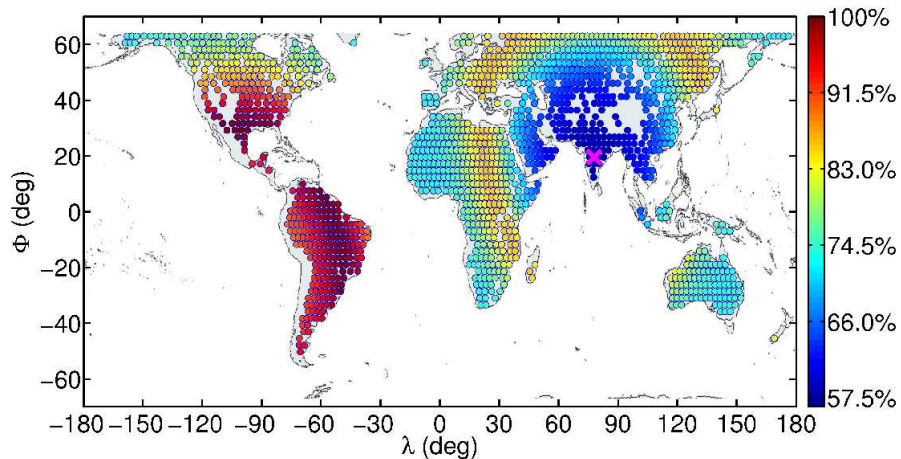


Figure 8: The colormap of  $C/C_{\max}$  values for 1524 different network configurations of two identical  $\Delta$ -telescopes, where  $C_{\max}$  is the highest value of the combined metric within the sample of 1524 elements. The location of the first telescope was chosen to be at  $[\Phi, \lambda] = [19.6^\circ, 78.0^\circ]$  (marked by  $\times$ ), and the location of the second telescope was chosen from the set of acceptable sites described in section 2.

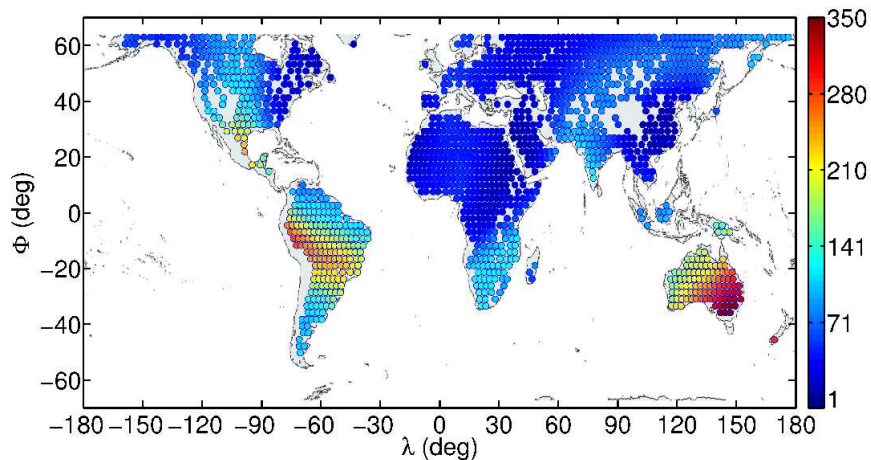


Figure 9: This colormap shows the number of acceptable sites within the annulus of optimal site locations for a second  $\Delta$ -telescope in a 2-telescope network, associated to the site location of the first telescope in the network. The map is calculated based on the 2-telescope combined ( $C$ ) metric results, where we found that the optimal sites for a second telescope form a  $\pm 7^\circ$  annulus at an angular distance of  $\sim 130^\circ$  from the location of the first telescope. The circles represent the acceptable site locations described in section 2, and their color represent the number of optimal site locations associated to them. The highest numbers (up to 350) of such optimal sites for a second telescope are associated to locations in Australia.

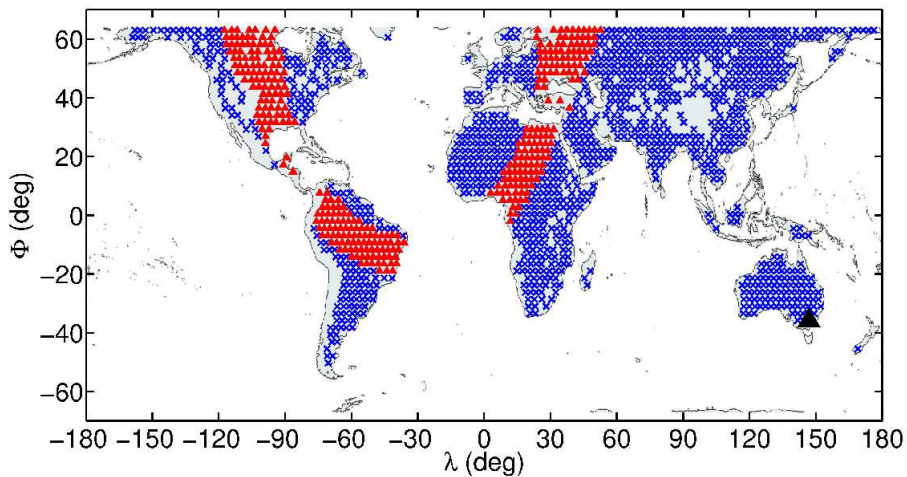


Figure 10: This map shows the annulus of the highest number of optimal site locations for a second  $\Delta$ -telescope in a 2-telescope network, together with the set of all acceptable sites described in section 2 ( $\times$  symbols). The annulus is formed by the set of optimal sites (represented by small triangles) derived from the combined ( $C$ ) metric map of a 2-telescope network where the first telescope is placed to  $[\Phi, \lambda] = [-35.8^\circ, 146.9^\circ]$  in Australia (represented by a big black triangle). Choosing a location in Australia (and the location at  $[\Phi, \lambda] = [-35.8^\circ, 146.9^\circ]$  in particular) for the site of the first  $\Delta$ -telescope provides the most options for optimal site selection when extending the network with a second instrument (see figure 9). In this case, the site location of the second  $\Delta$ -telescope of the network should be chosen from the elements of the annulus.

## 5. The LIGO-India case in the second generation GW detection network

In this analysis, we used a similar approach as for the  $\Delta$ -telescope networks to find the optimal location and orientation for the proposed LIGO-India detector within a five-detector network with Advanced LIGO (Hanford), Advanced LIGO (Livingston), Advanced Virgo, and KAGRA. In this case, we had taken into account in the calculation of the  $I$  and  $R$  metric that the LIGO-India is proposed to be a single L-shaped interferometer with 4 km long arms, similarly to the Advanced LIGO interferometers. Also, we used the assumption again that the strain sensitivity of all the interferometers in the network are practically the same.

We first created a new set of acceptable sites for LIGO-India by focusing our filtered map (see section 2) to the Indian region and by resampling the map with a higher ( $\sim 27$  km) resolution. The resulting discrete map of acceptable sites consisted of 5904 different geographical locations, covering whole India and even extending beyond the country.

We manually chose 3 site locations in India (in the Southern, in the North-Eastern and in the North-Western part of the country), and used each of them as a hypothetical site for LIGO-India. The orientation angle of the L-shaped interferometer was defined



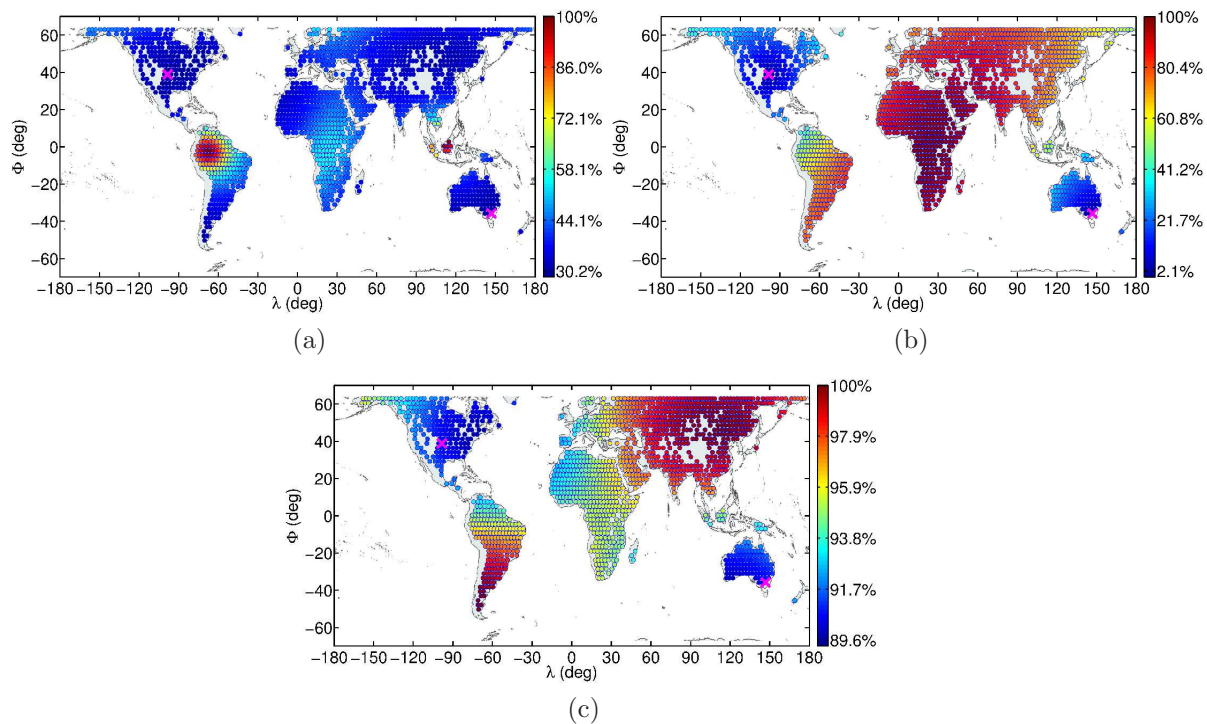


Figure 11: The colormaps of normalized metric values that we get for a network of three identical  $\Delta$ -telescopes in the case when one telescope is placed to  $[\Phi_{D1}, \lambda_{D1}] = [-35.8^\circ, 146.9^\circ]$  in Australia, and one to  $[\Phi_{D2}, \lambda_{D2}] = [38.9^\circ, -98.4^\circ]$  in North America (marked by  $\times$  symbols). The location of the third telescope is chosen from the set of acceptable sites described in section 2. Each circle in the maps corresponds to one of the 1523 site locations, while their colors represent the  $I/I_{\max}$  (a),  $D/D_{\max}$  (b), or  $R/R_{\max}$  (c) values, given in percentages, where the "max" indices correspond to the highest values of the three metrics within the samples of 1523 elements.

as the angle between the East direction and the bisector of the interferometer arms, measured counterclockwise. At each site, we calculated the  $I$ ,  $R$ ,  $D$ , and  $C$  metrics for every orientation angle from  $45^\circ$  to  $135^\circ$  with a resolution of  $0.1^\circ$ . Note, that the  $D$  metric is always independent from the orientation angle, and that the symmetry of projection of an incoming GW to the arms of an L-shaped interferometer makes it unnecessary to test any orientation angles below  $45^\circ$  and above  $135^\circ$ . Based on the results, the optimal orientation angle for LIGO-India was robustly found to be between  $57.7 - 58.9^\circ$  depending on the metric that we maximized ( $+k \times 90^\circ$  due to symmetry reasons with  $k$  being an integer).

In the case of site location optimization, instead of randomly choosing the site locations for LIGO-India, we carried out our analysis by testing all the 5904 different sites. Using each acceptable site in our list as a hypothetical location for LIGO-India, we calculated the  $I$ ,  $D$ ,  $R$ , and  $C$  metrics for the five-detector network, taking into account the known geographical positions and orientations of the Advanced LIGO Hanford and

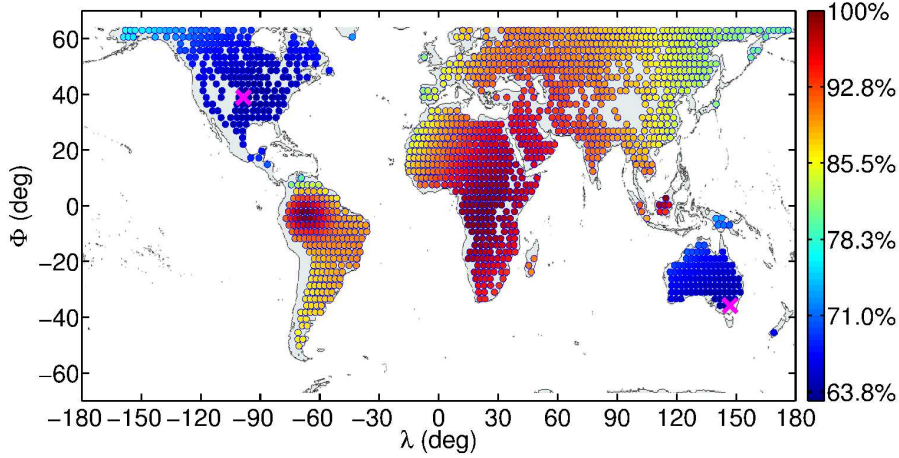


Figure 12: The colormap of  $C/C_{\max}$  values for 1523 different network configurations of three identical  $\Delta$ -telescopes, where  $C_{\max}$  is the highest value of the combined metric within the sample of 1523 elements. The location of the first telescope in the network were chosen to be at  $[\Phi_{D1}, \lambda_{D1}] = [-35.8^\circ, 146.9^\circ]$  in Australia, and at  $[\Phi_{D2}, \lambda_{D2}] = [38.9^\circ, -98.4^\circ]$  in North America (marked by  $\times$  symbols). The location of the third telescope was chosen from the set of acceptable sites described in section 2.

Livingston, Advanced Virgo, and KAGRA interferometers. The orientation angle for the LIGO-India interferometer was first set to be  $45^\circ$  and colormaps of  $I/I_{\max}$ ,  $D/D_{\max}$ ,  $R/R_{\max}$ , and  $C/C_{\max}$  values were produced, where the "max" indices corresponded to the highest value of the given metric within the sample of 5904 elements.

As we found that the  $I$ ,  $D$ , and  $C$  metric values are consistently higher in the Southern geographical regions, we repeated testing all the 5904 sites using an orientation angle of  $58.2^\circ$ , which we had found to be the optimal angle for a LIGO-India placed to the Southern part of India, based on the combined metric,  $C$ . The results are visualized in figure 15 for the three individual metrics, and in figure 16 for the combined metric. Note, that testing the different site locations using a  $45^\circ$  orientation angle resulted with very similar maps to the ones shown in figure 16, which shows that the optimal site locations within India are also very robust to the orientation angle of the interferometer.

Based on the  $I$ ,  $D$ , and the  $C$  metrics, we found that the rule of thumb is that the five-detector network of LIGO-India, Advanced LIGO Hanford and Livingston, Advanced Virgo, and KAGRA, becomes more and more optimal by placing LIGO-India more to the South within the Indian subcontinent. Even though the  $R$  metric favors the opposite geographical direction for the LIGO-India site, there is only a slight dependence of the network performance in terms of this metric.

As a final result, we chose an example for an optimal configuration for LIGO-India to have the site location at  $[\Phi = 10.02^\circ, \lambda = 77.76^\circ]$  and to have an orientation angle of  $58.2^\circ + k \times 90^\circ$  (see figure 17). The corresponding  $I/I_{\max}$ ,  $D/D_{\max}$ ,  $R/R_{\max}$ , and  $C/C_{\max}$  ratios (the "max" index corresponding to the highest values of the metrics within the



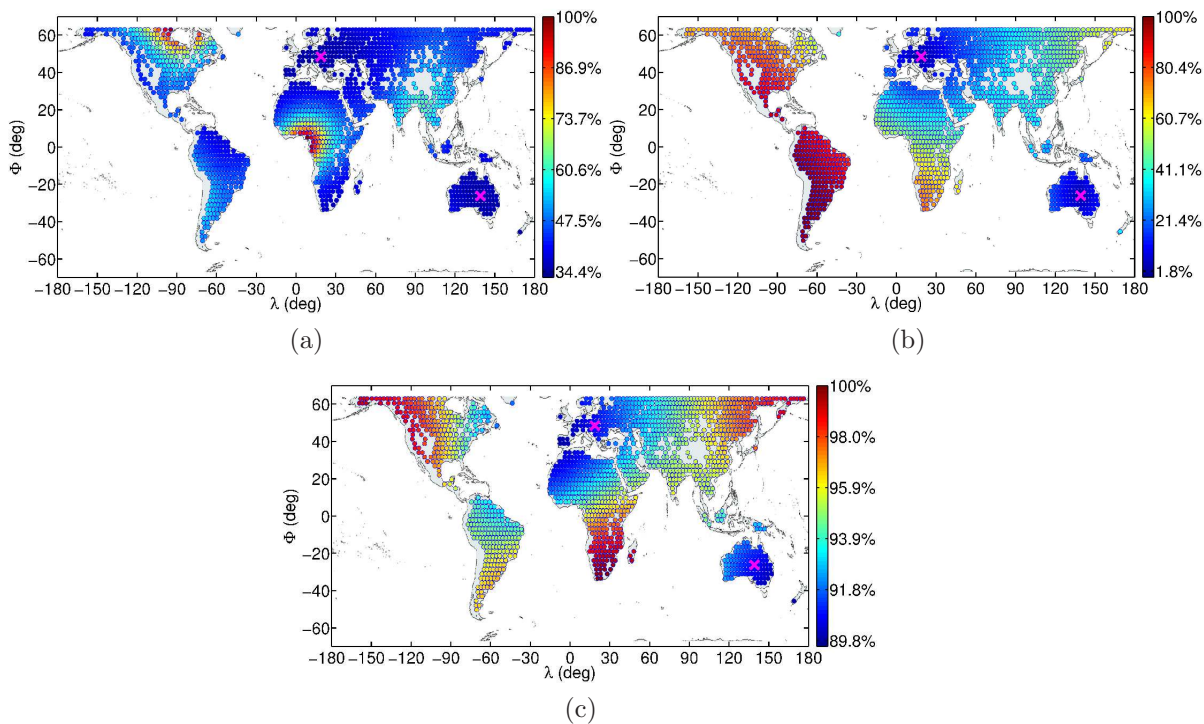


Figure 13: The colormaps of normalized metric values that we get for a network of three identical  $\Delta$ -telescopes in the case when one telescope is placed to  $[\Phi_{E1}, \lambda_{E1}] = [-26.2^\circ, 139.2^\circ]$  in central Australia, and one to  $[\Phi_{E2}, \lambda_{E2}] = [48.5^\circ, 18.7^\circ]$  in Europe (marked by  $\times$  symbols). The location of the third telescope is chosen from the set of acceptable sites described in section 2. Each circle in the maps corresponds to one of the 1523 site locations, while their colors represent the  $I/I_{\max}$  (a),  $D/D_{\max}$  (b), or  $R/R_{\max}$  (c) values, given in percentages, where the "max" indices correspond to the highest values of the three metrics within the samples of 1523 elements.

sample) as functions of the detector orientation angle are shown in figure 18. Note, that the dominant metric in terms of optimizing the orientation angle of the LIGO-India detector, is  $I$ , i.e. the capability of the network of reconstructing the polarization of a detected GW signal. This  $I$  metric can suffer even more than a  $\sim 25\%$  loss if the detector is not oriented optimally.

## 6. Discussion

In this section, we summarize the results presented in section 4 and 5, and suggest geographical regions where possible future  $\Delta$ -telescopes and the LIGO-India should be placed based on the  $N$ -telescope figures of merit we defined in section 3. We also suggest an optimal orientation for LIGO-India based on the same figures of merit.

The figures of merit we used to characterize and compare different configurations of  $N$ -telescope networks were the following (see section 3): (a) capability of reconstructing

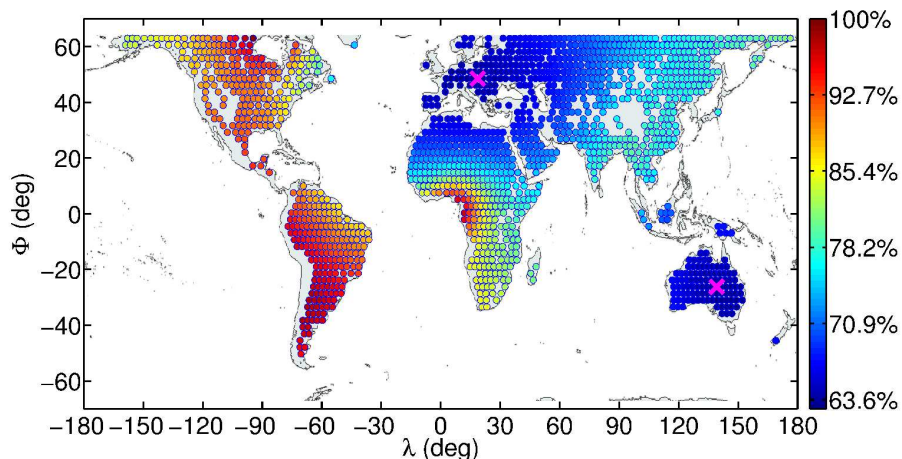


Figure 14: The colormap of  $C/C_{\max}$  values for 1523 different network configurations of three identical  $\Delta$ -telescopes, where  $C_{\max}$  is the highest value of the combined metric within the sample of 1523 elements. The location of the first telescope in the network were chosen to be at  $[\Phi_{E1}, \lambda_{E1}] = [-26.2^\circ, 139.2^\circ]$  in central Australia, and at  $[\Phi_{E2}, \lambda_{E2}] = [48.5^\circ, 18.7^\circ]$  in Europe (marked by  $\times$  symbols). The location of the third telescope was chosen from the set of acceptable sites described in section 2.

the polarization of a detected GW signal (measured by the  $I$  metric); (b) accuracy in localizing the GW source in the sky (measured by the  $D$  metric); (c) accuracy in reconstructing the parameters of a standard binary source (measured by the  $R$  metric). We also constructed a fourth metric (denoted by  $C$ ) that combines the  $I$ ,  $D$ , and  $R$  metrics with practically equal weight (see section 3.5).

In section 4 we calculated the  $I$ ,  $D$ ,  $R$ , and  $C$  maps in three example cases where the location of the first  $\Delta$ -telescope in a 2-telescope network was set to be in Europe (see figure 3 and 6), North America (see figure 4 and 7), and India (see figure 5 and 8), respectively. The maps were always normalized with the highest value of the different metrics within the sample of 1524  $I$ ,  $D$ ,  $R$ , and  $C$  values. Based on the combined metric results, we found that the optimal site locations for the second telescope in the network form a  $\pm 7^\circ$  annulus at an angular distance of  $\sim 130^\circ$  from the location of the first instrument. Using this result we calculated the number of acceptable sites within such annuli associated to all the acceptable sites, and found that the highest number of optimal sites correspond to locations in Australia (see figure 9). Thus, we conclude that placing the first telescope to Australia provides the most options (see figure 10) for optimal site selection when extending the network with a second instrument.

The site location for the second *Delta*-telescope in the network should be chosen from the set of acceptable sites within the annulus of optimal sites associated to the location of the first site. We chose two example cases of 3-telescope networks where the location of one telescope was chosen to be in Australia, and the second telescope was placed to North America (Example D; see figure 11 and 12), and to Europe (Example

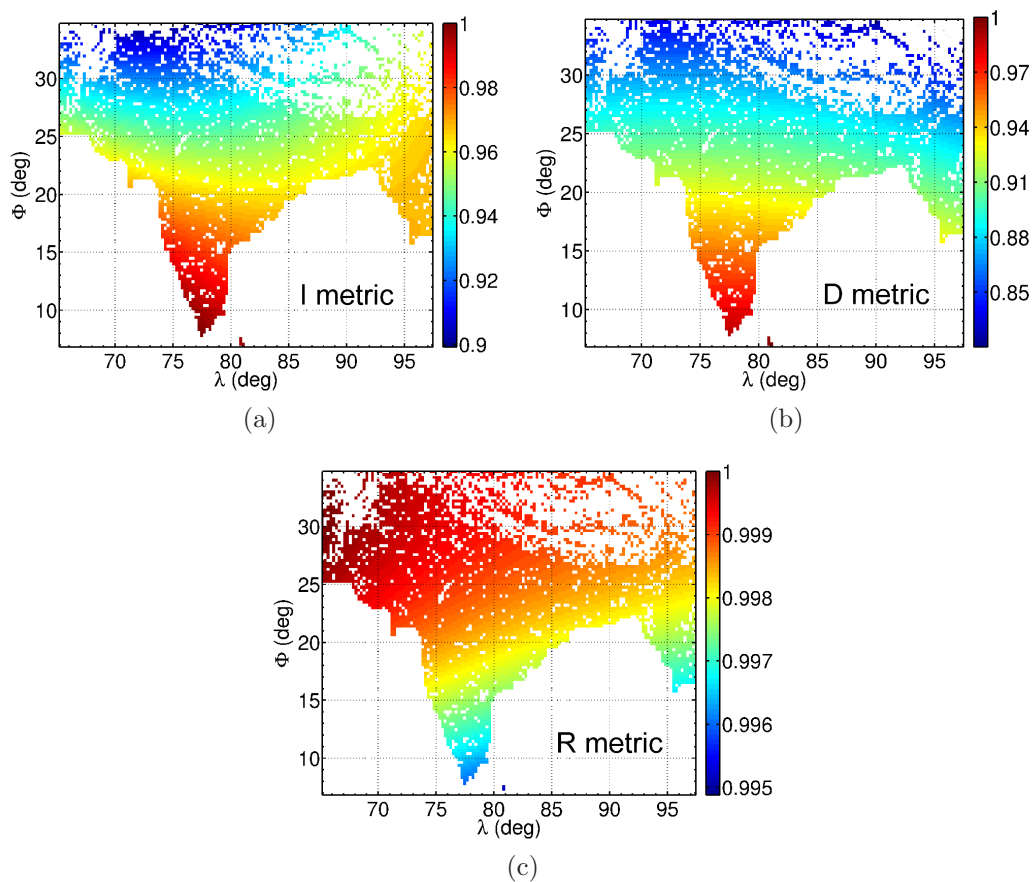


Figure 15: The colormaps of  $I/I_{\max}$  (a),  $D/D_{\max}$  (b), and  $R/R_{\max}$  (c) values in case of placing the LIGO-India site at different acceptable site locations in the Indian subcontinent. The "max" indices correspond to the highest value of the different metrics within the samples of 5904 elements. The orientation angle of the L-shaped interferometer (being the angle between the East direction and the bisector of the interferometer arms, measured counterclockwise) was optimized based on the  $C$  metric, and was set to be  $58.2^\circ$ . The optimal orientation angle was found to be robust in terms of the site location within India.

E; see figure 13 and 14), respectively. The optimal sites for a third telescope in such network was found to be on Borneo island and in the North-Central region in South America for Example D, and in North Canada and in West-Central Africa for Example E.

Using an India map of acceptable telescope sites with  $\sim 27$  km resolution, we tested a total of 5904 different site locations for LIGO-India, taking into account the Advanced LIGO Hanford and Livingston, Advanced Virgo, and KAGRA as further members of a five-detector network (see section 5). We found the optimal orientation angle of LIGO-India to be  $\sim 58.2^\circ + k \times 90^\circ$  ( $k$  being an integer) practically for all site locations within India, and based on the combined metric. Here, the orientation angle is defined

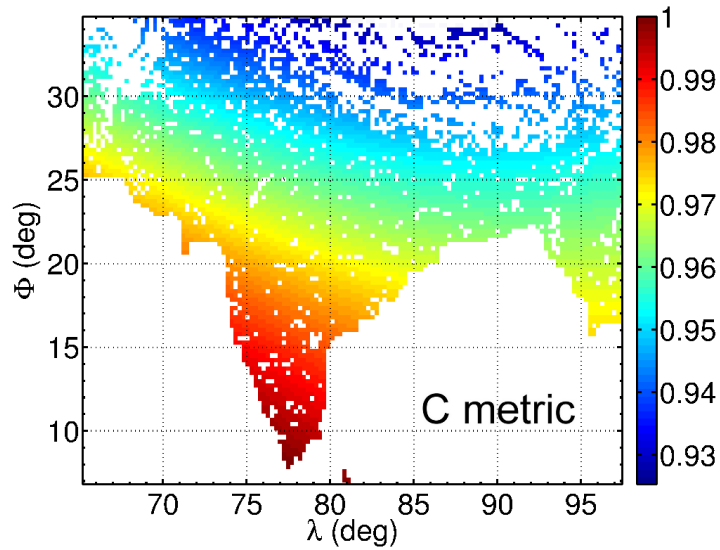


Figure 16: This figure shows the same results as figure 15 but for the  $C$  metric.

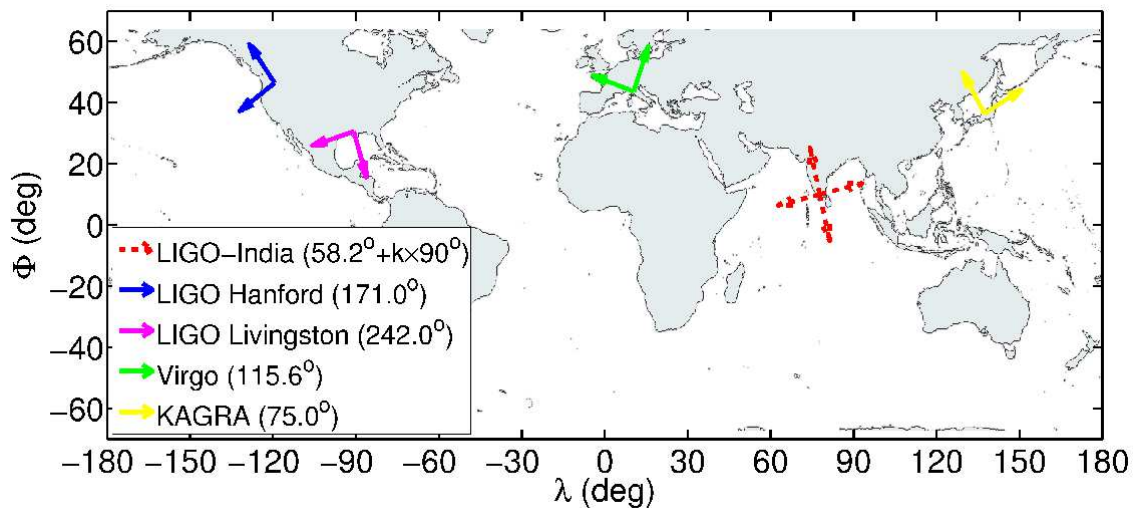


Figure 17: A suggested example for an optimal network of second generation GW detectors including LIGO-India. In this example the LIGO-India is placed to  $[\Phi = 10.02^\circ, \lambda = 77.76^\circ]$  with an orientation angle (being the angle between the East direction and the bisector of the interferometer arms, measured counterclockwise) of  $58.2^\circ + k \times 90^\circ$ ,  $k$  being an integer. The geographical positions and orientation angles of the other detectors in the network,  $([\Phi, \lambda]; \alpha)$ , were set to  $([46.4551^\circ, -119.41^\circ]; 171^\circ)$  for Advanced LIGO Hanford,  $([30.56^\circ, -90.77^\circ]; 242^\circ)$  for Advanced LIGO Livingston,  $([43.63^\circ, 10.5^\circ]; 115.6^\circ)$  for Advanced Virgo, and  $([36.42^\circ, 137.3^\circ]; 75^\circ)$  for KAGRA.

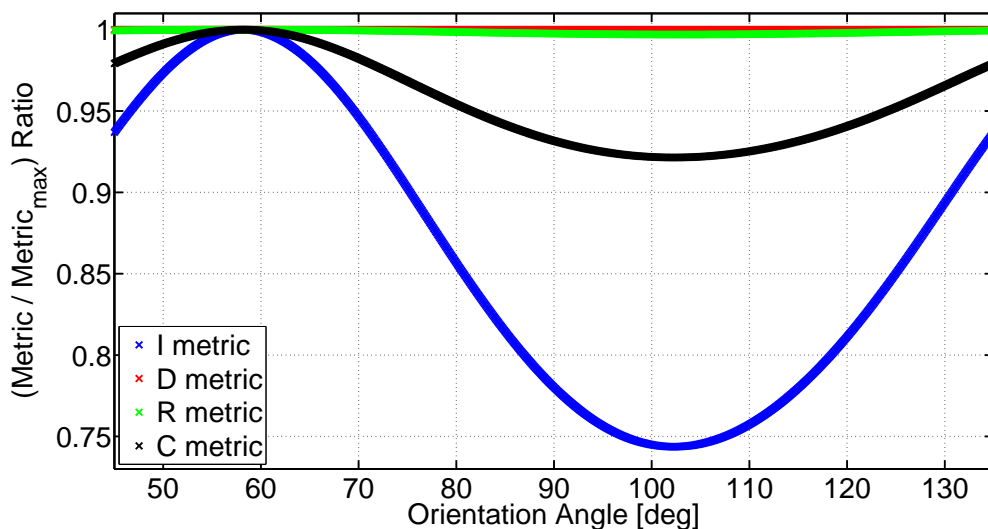


Figure 18: The  $I/I_{\max}$  (blue),  $D/D_{\max}$  (red),  $R/R_{\max}$  (green), and  $C/C_{\max}$  (black) ratios (the "max" index corresponding to the highest values of the metrics within the sample) as functions of the detector orientation angle for a hypothetical LIGO-India detector at a geographical location [ $\Phi = 10.02^\circ, \lambda = 77.76^\circ$ ]. Note, that the dominant metric in terms of optimizing the orientation angle is  $I$ , i.e. the capability of the network of reconstructing the polarization of a detected GW signal. This  $I$  metric can suffer even a  $\sim 25\%$  loss if the detector is not oriented optimally.

as the angle between the East direction and the bisector of the arms in the L-shaped interferometer, measured counterclockwise.

Also, by using an optimally oriented configuration, we found the Southern-Central part of India to be the most optimal region for the site of LIGO-India (probably the South-Eastern part of the Karnataka region, or North-Western part of the Tamil Nadu region; see figure 16). An example for an optimal location and orientation for LIGO-India is shown in Figure 17. Comparing the results shown in figure 15 and figure 18, we can also conclude that based on the network figures of merit, setting the orientation angle of the LIGO-India detector has greater significance than choosing the site location of the detector within India. In the optimization of the site location, the dominant term will be the source localization accuracy of the network ( $D$  metric), while in the optimization of the orientation angle, the dominant term will be the capability of the network of reconstructing the polarization of a detected GW signal ( $I$  metric).

More efforts are required in the future to overcome the limitations of the work presented here. Taking a lot more exclusionary criteria into account, possibly with continuously variable acceptance instead of the present yes/no type grid, would allow constructing a much more detailed and accurate set of acceptable sites. Applying public crowdsourcing in setting up a list of exclusionary criteria and/or inaccessible geographic areas would result with such a detailed map of possible constructions sites that probably



no group of researchers would be able to achieve.

Additional figures of merits can easily be added to the optimization process depending on the aim of various searches from GW transients to the stochastic GW background. One such figure of merit could be the expected duty cycle of the network or a sub-network of a given number of telescopes, as proposed by [14]. This figure of merit and potentially others could allow not only comparing different configurations of the same  $N$ -telescope network (as presented here) but also networks with different number of telescopes, leading to optimization of the number of telescopes in the network as well.

The  $I$ ,  $D$ , and  $R$  metrics have already been used in similar forms (without all-sky averaging) in previous works (see [16], [18], and [25]). These metrics can unquestionably be used to find the *optimal* configurations of  $N$ -telescope networks for all given  $N$ s, however any of them might need more elaboration if one wants to use them to make quantitative comparisons between optimal and sub-optimal configurations, or between networks of different numbers of telescopes. Also, one can use a different weighing of individual metrics when constructing the combined ( $C$ ) metric depending on the specific preferences one would like to follow, which might also be a subject to change with time as we move closer to the realization of future GW telescopes. These are all beyond the scope of this paper and should be investigated in a future follow-up paper.

Finally, the optimization of  $N$ -telescope networks could be based on regular or Markov chain Monte Carlo simulations using the set of acceptable sites and metrics. This would allow a more general testing of networks of  $N \geq 3$   $\Delta$ -telescopes. Also, as we pointed out in section 3, one could take into account the distribution of mass in the local Universe (e.g. using galaxy catalogs), and optimize the telescope network by maximizing the observational time with the highest directional sensitivity towards certain sky directions. We also leave these to be the scope of a future paper.

## Acknowledgments

This paper was reviewed by the LIGO Scientific Collaboration under LIGO Document P1200175. We'd like to thank Imre Bartos, Brian Dawes, Riccardo DeSalvo, Marco Drago, Sergei Klimenko, Gabriele Vedovato, Linqing Wen, and Stan Whitcomb for their valuable comments on the manuscript. The authors are grateful for the support of the LIGO-Virgo Collaboration, and Columbia University in the City of New York. This work has been supported by the United States National Science Foundation under cooperative agreement PHY-0847182, the Science and Technology Facilities Council of the United Kingdom, and the Scottish Universities Physics Alliance.

## References

- [1] B. P. Abbott et al. LIGO: the Laser Interferometer Gravitational-Wave Observatory. *Reports on Progress in Physics*, 72(7):076901, 2009.



- [2] T. Accadia et al. Virgo: a laser interferometer to detect gravitational waves. *Journal of Instrumentation*, 7:3012, 2012.
- [3] Advanced LIGO, <https://www.advancedligo.mit.edu/>.
- [4] Advanced VIRGO, <https://www Cascina.virgo.infn.it/advirgo/>.
- [5] B. Iyer et al. LIGO-India, Proposal of the Consortium for Indian Initiative in Gravitational-wave Observations (IndIGO). *LIGO-India Technical Report*, <https://dcc.ligo.org/cgi-bin/DocDB/ShowDocument?docid=75988>, 2011.
- [6] KAGRA, <http://gwcenter.icrr.u-tokyo.ac.jp/en/>.
- [7] J. Abadie et al. TOPICAL REVIEW: Predictions for the rates of compact binary coalescences observable by ground-based gravitational-wave detectors. *Classical and Quantum Gravity*, 27(17):173001, 2010.
- [8] ET Project, <http://www.et-gw.eu/>.
- [9] M. Abernathy et al. Einstein gravitational wave Telescope conceptual design study. *ET-0106C-10*, <https://tds.ego-gw.it/ql/?c=7954>, 2011.
- [10] M. Punturo et al. The Einstein Telescope: a third-generation gravitational wave observatory. *Classical and Quantum Gravity*, 27(19):194002, 2010.
- [11] A. Freise et al. Triple Michelson interferometer for a third-generation gravitational wave detector. *Classical and Quantum Gravity*, 26(8):085012, 2009.
- [12] E. Chassande-Mottin, M. Hendry, P. J. Sutton, and S. Márka. Multimessenger astronomy with the Einstein Telescope. *General Relativity and Gravitation*, 43(2):437–464, 2011.
- [13] NASA Visible Earth, <http://visibleearth.nasa.gov/view.php?id=55167>.
- [14] B. F. Schutz. Networks of gravitational wave detectors and three figures of merit. *Classical and Quantum Gravity*, 28(12):125023, June 2011.
- [15] R. Weiss et al. Report of the Committee to Compare the Scientific Cases for Two Gravitational-wave Detector Networks: (AHLV) Australia, Hanford, Livingston, VIRGO; and (HHLV) two detectors at Hanford, one at Livingston, and VIRGO. *Technical report*, 2010.
- [16] S. Klimenko et al. Localization of gravitational wave sources with networks of advanced detectors. *Physical Review D*, 83(10):102001, 2011.
- [17] M. Drago. Search for Transient Gravitational Wave Signals with Unknown Waveform in the LIGO VIRGO Network of Interferometric Detectors Using a Fully Coherent Algorithm. *PhD thesis, Università degli Studi di Padova*, 2010. [https://atlas3.atlas.aei.uni-hannover.de/~drago/LSC/Documents/Drago\\_XXII-PhD-thesis.pdf](https://atlas3.atlas.aei.uni-hannover.de/~drago/LSC/Documents/Drago_XXII-PhD-thesis.pdf).
- [18] S. Fairhurst. Source localization with an advanced gravitational wave detector network. *Classical and Quantum Gravity*, 28(10):105021, 2011.
- [19] L. Wen and Y. Chen. Geometrical expression for the angular resolution of a network of gravitational-wave detectors. *Physical Review D*, 81(8):082001, 2010.
- [20] C. Cutler and É. E. Flanagan. Gravitational waves from merging compact binaries: How accurately can one extract the binary’s parameters from the inspiral waveform? *Physical Review D*, 49:2658–2697, 1994.
- [21] C. Moreno-Garrido, J. Buitrago, and E. Mediavilla. Spectral Analysis of the Gravitational Radiation Emitted by Binary Systems in Moderately Eccentric Orbits - Application to Coalescing Binaries. *Monthly Notices of the Royal Astronomical Society*, 266:16, 1994.
- [22] A. Albrecht et al. Findings of the Joint Dark Energy Mission Figure of Merit Science Working Group. *arXiv:0901.0721*, 2009.
- [23] J. T. Whelan. Stochastic Gravitational Wave Measurements with Bar Detectors: Dependence of Response on Detector Orientation. *LIGO Document P050041-00-Z*, 2005.
- [24] B. Kocsis et al. Premerger localization of gravitational-wave standard sirens with LISA: Harmonic mode decomposition. *Physical Review D*, 76(2):022003, 2007.
- [25] P. Ajith and S. Bose. Estimating the parameters of nonspinning binary black holes using ground-based gravitational-wave detectors: Statistical errors. *Physical Review D*, 79(8):084032, 2009.